2023 IEEE International Conference on Robotics and Automation (ICRA 2023)
May 29 - June 2, 2023. London, UK

Design Optimization and Data-driven Shallow Learning for Dynamic Modeling of a Smart Segmented Electroadhesive Clutch

Navid Feizi[1], Zahra Bahrami[2], S. Farokh Atashzar[3], Mehrdad R. Kermani[4], Rajni V. Patel[5]

Abstract— **Electroadhesive clutches have attracted a great deal of interest in the last decade as semi-active actuators for human-robot interaction due to their lightweight, low power consumption, and tunable high-torque output capability. However, because of the complexity of their dynamics, in most cases, they are utilized in an ON/OFF-control strategy. In this regard, the non-autonomous (time-dependent) degradation of electroadhesive behavior is an inherent challenge that injects unpredictability and uncertainty into the behavior of this family of semi-active clutches. We propose a novel approach to preventing degradation of electroadhesion using a segmented electrode design that modulates the electrical field on the dielectric surface while using a direct current signal and securing low power consumption. This paper, for the first time, presents an optimization process based on a novel analytic model of the proposed actuator. It also develops a data-driven model augmentation using a hybrid shallow learning approach composed of a long short-term memory (LSTM) architecture which is combined with the analytical model. The performance of the proposed semi-active clutch and the data-driven hybrid model is experimentally validated in this paper.**

I. INTRODUCTION

Human-centered robotic systems have attracted a great deal of interest in various industries, including in the medical domain and in automotive factories. Such robots share a large workspace with humans; thus, their inherent safety is of paramount importance [1]–[5]. In order to satisfy the safety requirements, several software techniques are proposed in the literature, including passivity-based stabilizers besides, fault-detection, and fault-tolerant control [6]. Despite the benefit of software safety, it is always required to have a mechanical safety layer to avoid safety violations in case a dangerous event is not detected or avoided due to software glitches. Mechanical safety features are typically achieved through decoupling high impedance actuators from the end effector or employing semi-passive actuators that provide inherent safety in the system [7].

Magneto-rheological (MR) and electro-rheological (ER) clutches are two of the common semi-passive actuators that have been widely used in human-robot interaction (HRI) systems [8], [9]. Both of these systems generate a tunable mechanical coupling between the actuator and the end effector through viscous friction. In an MR clutch, the transferred torque (or transferred force in a linear design) can be controlled by varying the magnetic field around the smart MR fluid inside the clutch. Despite the significant performance improvement in terms of torque density that is achieved using permanent magnets [10] and squeeze mode design [11], MR clutches are heavy and consumes high-power. The transferred torque of an ER clutch is controlled by varying the electric field applied to the driving ER fluid. This can be achieved with lightweight components [9]. However, the naturally low viscosity of the ER fluid limits the transferred torque of the clutch. The above-mentioned issues limit the application of ER and MR clutches in mobile and/or wearable HRI systems [12].

Electroadhesion (EA) actuators provide a higher force density when compared with the ER- and MR-based actuators. EA has been used mostly for pick and place applications and wall climbing robots [13], [14]. The proper selection of dielectric and substrate materials results in very high adhesion with low energy consumption. The friction force due to this adhesion has been used as an ON/OFF locking mechanism. A tubular EA clutch was used in a variable stiffness wing skeleton in [15]. In [16], and [17], linear EA clutches have been used to develop wearable tactile devices. A lightweight, low-power linear EA clutch is used in [18] for an ankle exoskeleton. The same group also investigated the effect of the design parameters on EA [19]. Electroadhesion is used to lock the revolute joints of a robotic hand [20] and the prismatic joints of a tactile display [21]. The effectiveness of the EA clutches in rehabilitation and assistive robotics has been evaluated in our prior work [22], [23].

One of the primary challenges of electroadhesion is the accumulation of space charge in the dielectric material over

The work of NF and RVP was funded by the Natural Sciences and Engineering Research Council (NSERC) of Canada under grant #RGPIN-1345 (awarded to RVP) and the Tier-1 Canada Research Chairs Program (RVP). The work of MRK was funded by NSERC under grant #RGPIN-06253. The work of SFA is supported by the US National Science Foundation under Grant 2121391 and Grant 2208189; also in part by NYUAD Center for Artificial Intelligence and Robotics under Award CG010.

[1]Navid Feizi (corresponding author) is with Canadian Surgical Technologies and Advanced Robotics (CSTAR), Lawson Health Research Institute, London, ON N6A 5A5, Canada, and with the School of Biomedical Engineering, Western University, London, ON N6A 3K7, Canada (email: nfeizi@uwo.ca)

[2]Zahra Bahrami is with the Institute of Geography, University of Erlangen-Nuremberg, 91054 Erlangen, Germany. (email: Zahra.bahrami@fau.de)

[3]S. Farokh Atashzar is with the Department of Mechanical and Aerospace Engineering, the Department of Electrical and Computer Engineering, and the Department of Biomedical Engineering, New York University (NYU), New York, NY 10003 USA. He is also with NYU WIRELESS and NYU CUSP. (email: f.atashzar@nyu.edu)

[4]Mehrdad R. Kermani is with the Department of Electrical and Computer Engineering, Western University, London, ON N6A 5B9, Canada (email: mkermani@eng.uwo.ca)

[5]Rajni V. Patel is with Canadian Surgical Technologies and Advanced Robotics (CSTAR), Lawson Health Research Institute, London, ON N6A 5A5, Canada, and with the Department of Electrical and Computer Engineering, the School of Biomedical Engineering, the Department of Surgery, and the Department of Clinical Neurological Sciences, Western University, London, ON N6A 5B9, Canada (email: rvpatel@uwo.ca)

time, which counteracts the primary electric field. This leads to electroadhesion degradation while the clutch is in operation, and slows down de-adhesion after deactivation, resulting in residual adhesion [22], [24]–[27]. The utilization of reversing polarity and resonant vibration of the disc at the onset of deactivation for the swift release of electroadhesion was explored in [28]. Our prior research has investigated the effect of the continuous use of an alternating current (AC) signal during the activation of electroadhesion clutches to eliminate residual adhesion caused by space charges [22], [23]. However, the proposed solutions resulted in noise generation, as well as a higher current. Electroadhesion degradation has not been investigated extensively in the literature, mainly because electroadhesion has only been employed in ON/OFF applications, mostly for short durations, allowing the space charges to disappear during the inactive phases.

In this paper, we propose the design, implementation, and modeling of a novel segmented electrode design (SED) for a torque-tunable rotary electroadhesive clutch. The proposed SED approach modulates the electric field at the surface of the dielectric, which results in the elimination of torque degradation and residual torque. An optimal design of the clutch is presented based on an analytical model developed in this paper for the first time. The analytic optimization is utilized to implement the clutch. In addition, a hybrid data-driven model was also proposed that enhances the analytic modeling to take into account the unmodeled dynamics and implement a hybrid shallow learning pipeline that can predict the behavior of the proposed design. The hybrid model functions based on the fusion of the analytical model and long short-term memory (LSTM) architecture and will model the hidden nonlinear dynamics of the proposed clutch. Due to the controllable functionality and accuracy of the proposed model, this class of actuators can have high applicability in HRI systems, including mobile and wearable robots, and can offer lightweight and low power control.

II. DESIGN

The electroadhesion between two conductors follows Coulomb's law. The attraction stress between two parallel conductor electrodes separated by a dielectric is given by

$$\sigma_{sh}(V) = \frac{\varepsilon_r \varepsilon_0 V^2}{2h^2} \tag{1}$$

where ε_r is the relative permittivity of the insulator, ε_0 is the permittivity of vacuum, V is the applied voltage across the plates, and h is the distance between the plates.

In (1), the effect of charge buildup in the dielectric, which leads to adhesion degradation, is neglected. The charge buildup with a direct current (DC) signal can be formulated with an exponential decay function [24], thus, leading to the step response of the resultant shear stress as follows:

$$\sigma_{sh}^{DC}(t,V) = \sigma_{sh}(V) - \sigma_{sh}(V)\left(1 - e^{-t/\tau_d}\right) \tag{2}$$

where τ_d is the time constant of the degradation function. The first and the second terms in (2) represent stress due to the primary electric field, and the adhesion degradation due to charge buildup, respectively.

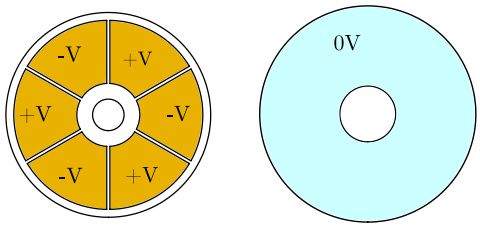

Fig. 1. Schematic of the SED stator (left) and the rotor (right) discs.

A. Segmented Electrode Design Concept

By modulating the electric field using the SED design, the direction of the electric field gradually flips with the rotation of the rotor. The gradual change of the electric field prevents EA degradation. To do so, both positive and negative electrodes are placed on one of the discs (we selected the stator disc in this paper), which is not covered with the dielectric. The conductor part of the stator disc is segmented into smaller parts with a uniform gap between them. Every other segment of the stator disc is connected together, creating two classes of segments. One class is charged positive, and the other one is charged negative, as shown in Fig. 1. The rotor disc, which slides against the stator disc, is made of a uniform conductor covered with dielectric and has relative voltage potential of zero.

Putting the stator disc and the rotor disc against each other leads to the electric field, as shown in Fig. 2, over the dielectric. As can be seen, with relative rotation of the discs, the direction of the electric field over the dielectric flips. This gradual change in the dielectric field prevents residual charge buildup in the field without the need for alternating the voltage across the electrodes.

B. Optimal design

Increasing the modulation frequency of the electric field by increasing the number of segments results in less EA degradation and, therefore, higher torque. However, the number of gaps between segments also increases with the increase of the number of segments. Therefore, the effective area of the discs, which only includes the area of the electrodes, and thus the maximum output torque, reduces. Reducing gap width increases the effective area of the disc, but it also limits the

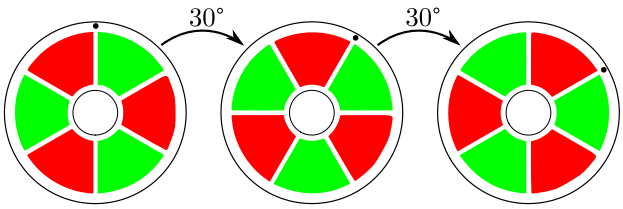

Fig. 2. Electric field over the dielectric. Red color denotes the electric field going into the plane and green color denotes the electric field coming out of the plane.

applied voltage across the electrodes due to electric discharge between two adjacent positive and negative electrodes. This trade-off demonstrates the need for the optimal design of the number of segments.

In order to find the optimal design to achieve the maximum torque, the equation of the torque should be calculated. By considering an infinitesimal portion of the dielectric on the rotor disc with radius r and angular position θ in polar coordinate, as shown in Fig. 3, and integrating the torque over the friction area, the equation for the maximum achievable torque is obtained as follows:

$$T(t) = \int_0^{2\pi} \int_{r_1}^{r_2} r C_f dF_n \tag{3}$$

where r_1 and r_2 are the inner and outer radii of the friction ring, C_f is the friction coefficient, and dF_n is the normal force applied to the infinitesimal piece due to adhesion which is given by

$$dF_n = E^2 \varepsilon_0 \varepsilon_r r dr d\theta \tag{4}$$

where E is the resultant electric field associated with the infinitesimal piece, ε_0 is the permittivity of vacuum, ε_r is the relative permittivity of the dielectric, and the resultant electric field E over the dielectric is given by

$$E = E_p + E_s \tag{5}$$

where E_p is the primary electric field given by

$$E_p = \frac{V(\theta, r, v)}{h} \tag{6}$$

and E_s is the electric field due to the space charge buildup. According to the step response mentioned in (2), E_s is formulated by the differential equation below:

$$\dot{E}_s + \frac{E_s}{\tau_d} + \frac{V(\theta, r, v)}{\tau_d h} = 0 \tag{7}$$

where τ_d is the time constant of the electric field degradation, h is the thickness of the dielectric, and V is the voltage difference across the two electrodes over the dielectric piece. Voltage for a point with radius r and angle θ for the geometry of the proposed SED is determined as follows:

$$V(\theta, r, v) = \begin{cases} 0 & \theta_1(r) > \theta_i \geq 0 \quad (8a) \\ v & \theta_2(r) > \theta_i \geq \theta_1(r) \quad (8b) \\ 0 & \theta_3(r) > \theta_i \geq \theta_2(r) \quad (8c) \\ -v & \theta_4(r) > \theta_i \geq \theta_3(r) \quad (8d) \\ 0 & \theta_b > \theta_i \geq \theta_4(r) \quad (8e) \end{cases}$$

where

$$\theta_i \equiv \theta \bmod \theta_b \tag{9}$$

in that θ_b is the associated angle for a block including a pair of electrodes which is equal to $\frac{720}{N}$ where N is the number of segments and is an even number; θ is the absolute angle of the infinitesimal piece, which is given by

$$\theta = \int_0^t \omega(t) + \phi_0 \tag{10}$$

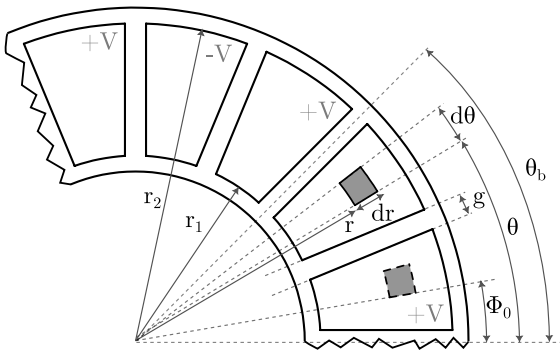

Fig. 3. Dimension of a piece of segmented disc and the infinitesimal piece.

where ω is the relative rotational velocity of the rotor disc with respect to the stator disc at time t, and ϕ_0 is the initial angle of the piece; $\theta_1(r)$ to $\theta_4(r)$ represent the boundary of a pair of electrodes for radius r and are given by

$$\theta_1(r) = f(g,r), \quad \theta_2(r) = \frac{\theta_b}{2} - f(g,r) \tag{11a}$$

$$\theta_3(r) = \frac{\theta_b}{2} + f(g,r), \quad \theta_4(r) = \theta_b - f(g,r) \tag{11b}$$

where

$$f(g,r) = \sin^{-1}\left(\frac{g}{2r}\right) \tag{12}$$

and g is the width of the gap between the electrodes.

The electric field given by the analytical model (5) was numerically calculated over the whole friction area for a 6-segment rotor using MATLAB. In this simulation, the voltage difference between the electrodes was 400 V, which resulted in 200 V between the electrode and the rotor disc. The simulation parameters are shown in Table I. Fig. 4 shows the resultant electric field at the onset of activation of the clutch (left figure) and after 10 seconds of activation when the rotor rotates with 2 RPM (right figure). As seen, the electric field degrades gradually from head to tail of each segment after a passage of time. However, the modulation of the electric field when a segment with an opposite charge slides against a part of the dielectric with accumulated space charge increases the resultant electric field to the maximum.

The electric field degradation time constant τ_d was selected based on measurements in the preliminary experiments. The friction coefficient C_f was selected based on the

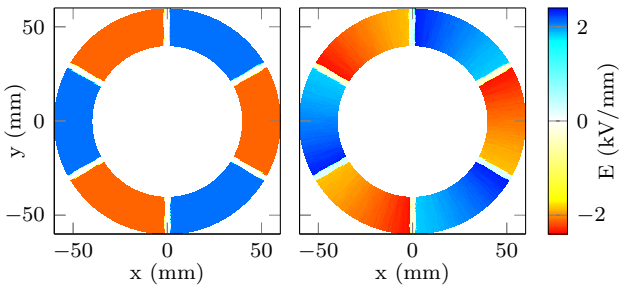

Fig. 4. Left: electric field around the dielectric at t = 0 s. Right: electric field around the dielectric at t = 10 s.

TABLE I

SIMULATION PARAMETERS

parameter	value	parameter	value	parameter	value
τ_d	10 s	ε_r	32	r_1	40 mm
C_f	0.28	h	95 μm	r_2	60 mm

experimental measurement of the friction of dielectric against steel [23]. The dielectric thickness h is selected to be $95\mu m$, which is thicker than the optimal value reported in [19]. A thicker dielectric layer increases the lifespan of the clutch due to wear and also provides stronger electric isolation between the discs. According to the air breakdown electric field threshold (3 kV/mm), the air gap between two adjacent electrodes should be larger than 0.33 mm to avoid electric discharge between the two adjacent electrodes with a 1 kV voltage difference (the maximum applicable voltage limited by the electronics). However, the preliminary experiments have shown that a large safety factor should be considered in the design since the accumulation of the debris in the gap between electrodes causes electric discharge at a much lower voltage than expected. Thus, the gap between electrodes was selected to be 2 mm.

The maximum output torque of the clutch formulated in (3) when the clutch is activated with a step signal is shown in Fig. 5 (results are for one friction ring). The transition of the electric field from uniform to decayed, as shown in Fig. 4, has led to an under-damped behavior of the torque. As seen, the number of segments and the velocity of rotation has a direct effect on the frequency of oscillation of the torque.

The design velocity range of the clutch was selected to be 0.5 RPM to 15 RPM. The average of the maximum achievable torque for a number of segments ranging from 4 to 40 is calculated using (3). The results are shown in Fig. 6. It has been observed that the torque increases with the decrease in the number of segments when velocity is high. However, due to the non-monotonic behavior of the

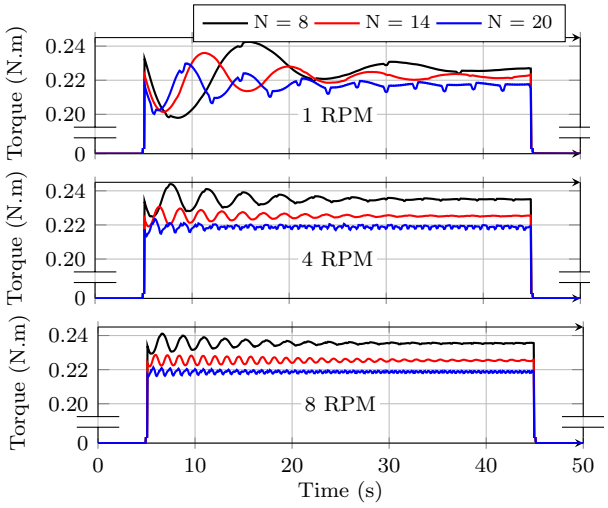

Fig. 5. Torque vs time for different velocities and number of segments. The clutch was activated for 40 seconds with 200 V with a Step signal.

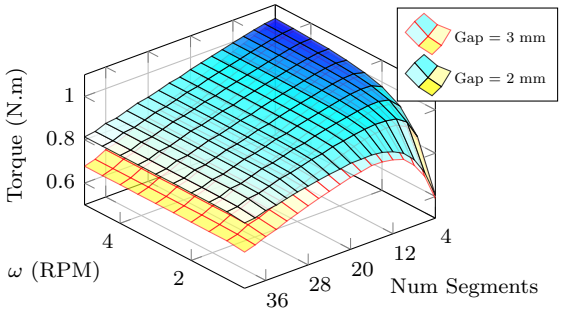

Fig. 6. Effect of the number of segments and velocity on the maximum torque.

torque with changes in the number of segments at lower velocities, the lower bound of the velocity span, 0.5 RPM, has been selected as the basis for design optimization. As a consequence, the optimal number of segments was determined to be 14. Furthermore, to demonstrate the impact of the gap width, the same results are also presented for a gap width of 3 mm. As observed, there is a reduction in torque output with the increase in gap width.

III. FABRICATION

The rotor disc was made of a 0.1 mm thick 1059 Spring steel sheet covered with five layers (95 μm thick) of Dupont 8153 dielectric. The sheet was cut to shape using electric discharge machining, as shown in Fig. 7. The inner diameter of the rotor disc was selected to be 8 cm.

The stator disc was made of a 2-layer circular printed circuit board (PCB) with an outer diameter of 12 cm. Every other electrode on the disc is connected together, and the electrodes on each side of the disc are connected to the associate electrode on the other side of the disc. A constant gap of 2 mm was maintained between adjacent electrodes. However, the gap was reduced to 1.2 mm out of the friction area to discharge the electrodes without damaging the dielectric in case of an unexpected high voltage. In order to increase the friction area, one stator disc is sandwiched between two rotor discs.

A custom PCB was made to activate the clutch. A 1 kV MHV 12 DC-DC high voltage transformer (Bellnix Co.,

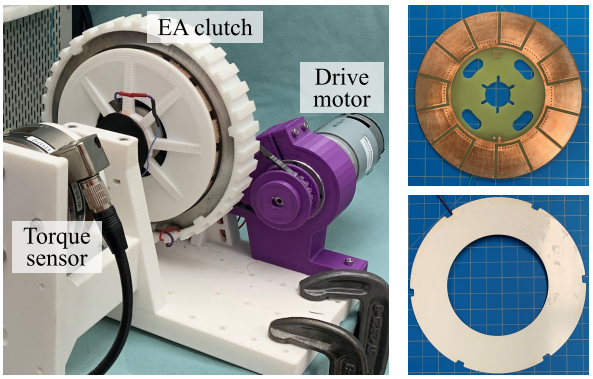

Fig. 7. Left: EA clutch test setup. Right: stator and rotor discs.

Saitama, Japan) was used to provide the required voltage. An MCP4821 digital-to-analogue converter chip (Microchip Technology, AZ, US) was used to adjust the output voltage of the transformer, and Arduino was used to interface the driver circuit to QuaRC software (Quanser, ON, Canada) in the MATLAB Simulink environment through serial communication.

IV. DATA-DRIVEN MODEL

The analytical model proposed in Section II covered the general dynamic behavior of the clutch and was used to optimize the design of the segmented clutch. However, the accuracy of the torque estimation of the analytical model is compromised by the unmodeled nonlinear dynamic of the clutch. In this section, a fusion of the proposed analytical model with an LSTM network is proposed, resulting in a hybrid data-driven approach to significantly boost the accuracy of the clutch model, taking advantage of the power of the LSTM in modeling dynamical behavior through learning while also taking into account the known part of the dynamics through analytical modeling.

The analytical part of the model can provide robustness in case the collected data does not train the full analytical behavior of the system. In addition, the LSTM would allow covering complex temporal behavior such as the hysteresis of the system using the internal memory components. LSTM has been used in the literature to model the dynamics of other complex actuators [29]–[31]. Each LSTM layer is consisted of forgetting, update, and output gates that learn to adjust the flow of information from the past hidden state to the future state and pass the relevant information downstream [32]. The equations of an LSTM block are as follows:

$$a^{<t>} = \Gamma_o * \tanh\left(c^{<t>}\right) \tag{13a}$$

$$c^{<t>} = \Gamma_u * \tilde{c}^{<t>} + \Gamma_f * c^{<t-1>} \tag{13b}$$

$$\tilde{c}^{<t>} = \tanh\left(w_c[a^{<t-1>}, X^{<t>}] + b_c\right) \tag{13c}$$

$$\Gamma_u = \sigma\left(w_u[a^{<t-1>}, X^{<t>}] + b_u\right) \tag{13d}$$

$$\Gamma_f = \sigma\left(w_f[a^{<t-1>}, X^{<t>}] + b_f\right) \tag{13e}$$

$$\Gamma_o = \sigma\left(w_o[a^{<t-1>}, X^{<t>}] + b_o\right) \tag{13f}$$

where Γ_u, Γ_f, and Γ_o denote the update gate, the forgetting gate, and the output gate, respectively; a is the output of the previous block; w_x and b_x are the trainable weights and biases for the associated gate; and X is the input time sequence.

A. Data Collection

In order to train the network, a 30-minute sequence of velocity, voltage, and torque data was recorded with a sampling frequency of 100 Hz. During the data collection procedure, the rotor of the clutch was rotated with a random velocity from 1 to 10 RPM and for a random duration. The clutch was activated with a random amplitude of 0 to 350 V and for a random duration. Fig. 8 shows a sample of the training data.

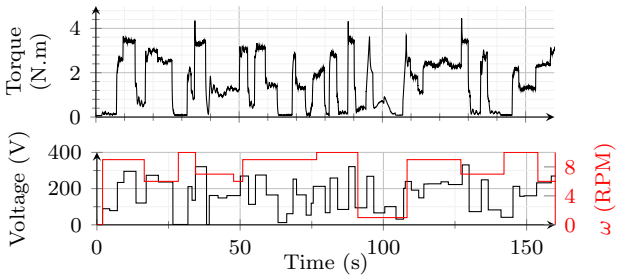

Fig. 8. A sample of the training data vs time.

B. Network Structure

A many-to-one network made of 5 LSTM layers with 100 nodes for each layer and one fully-connected (dense) layer was used. The analytical model estimation y was merged with the input signals (voltage V and velocity ω) before the LSTM network, as shown in Fig 9.

The mean square error (MSE) was used to calculate the loss between prediction and ground truth. Adam optimization was used to update the weights of the network (learning rate = 0.005). The learning rate, the number of hidden layers, the number of nodes per layer, and the location of the merged layer were manually tuned through observation of the effect of each parameter in minimizing the training loss. The model was implemented using the TensorFlow open-source library in Python and was trained for 1000 epochs. The MSE for the training data was determined to be 6.7×10^{-4} N.m. Fig. 10 shows the training loss.

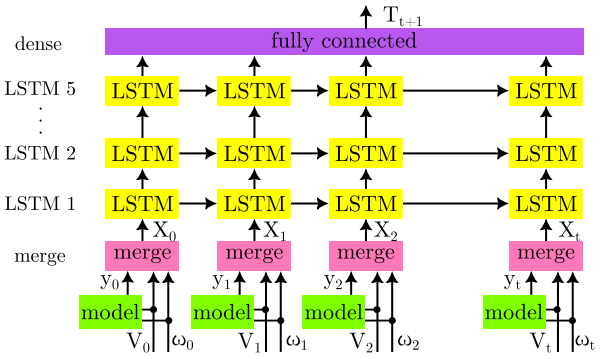

Fig. 9. LSTM Network.

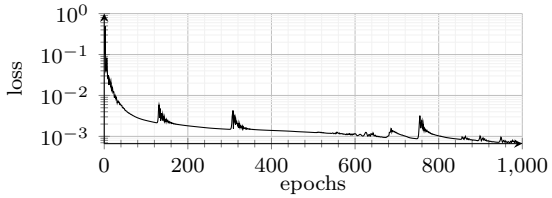

Fig. 10. Training loss vs epochs.

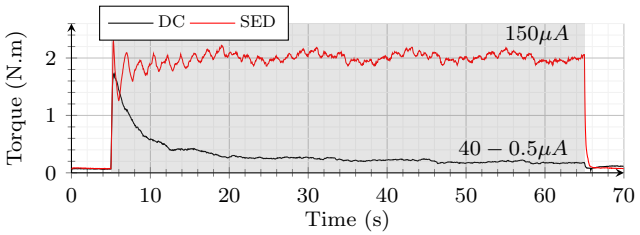

Fig. 11. Torque vs time for conventional DC mode and SED. The clutch was active in the area shaded in gray.

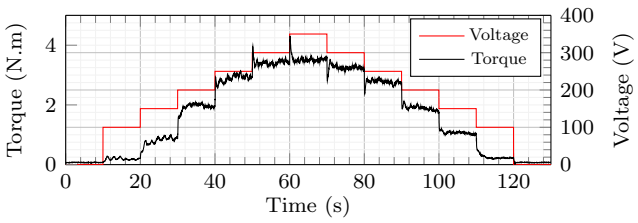

Fig. 12. Torque vs time for stairs input signal.

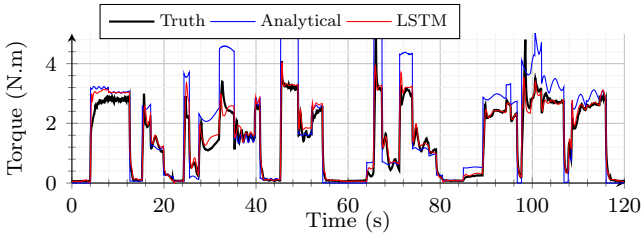

Fig. 13. Analytical model, LSTM prediction, and the truth value for a part of the test data.

V. Results and Discussion

Fig. 11 shows the results when the clutch was activated with conventional DC and the proposed segmented DC method. In both experiments, the same rotor and stator disc were used to allow comparison of the three modes. In the conventional DC mode, all segments of the stator disc were connected together, and the clutch was activated with 200 V. In the segmented DC mode, 200 V was applied between each segment and rotor disc (400 V across adjacent segments). The numbers close to each graph in Fig. 11 show the electric current used during each experiment. In all experiments, the rotor was rotated at 5 RPM.

As can be seen, the torque degrades significantly with time for DC activation. However, the proposed SED results in maintaining a torque much more than the DC mode. By comparing the experimental results with the analytical model presented in Section II, it can be seen that the under-damped behavior in the experiment complies with the analytical model results shown in Fig. 5. This behavior is due to the transition of the uniform electric field to the modulated electric field, as shown in Fig. 2.

Fig. 12 shows the output torque for a stairs input signal with the amplitude of 100 to 350 V. As can be seen, the average torque nonlinearly increases with the increase of the input voltage. An under-damped behavior can also be seen for low voltages; however, it damps out after a while for high voltages. We cannot provide a reasonable explanation for the vanish of the under-damped behavior with time. In addition, spikes can be seen in the torque signal at the onset of change of the signal in high voltages. This is mainly because of the instantaneous static friction between the discs (which is more than sliding friction) when the voltage and, consequently, the friction are high. It was observed that the width of the spikes reduces with the increase of velocity, and also, the dynamics of torque change with the change of velocity. These variations with torque with velocity are because of the inherent dependency of the electric field on velocity and also the variation in friction with change in velocity. Thus, other nonlinear dynamics are involved in the system, which are not considered in the model.

Fig. 13 shows the analytical model, the hybrid LSTM network predictions, and the ground truth value for 2 minutes of the testing dataset. The testing dataset was recorded when the clutch was rotated with a random velocity, and the clutch was activated with step signals with random amplitude and random duration, similar to the training dataset. As can be seen, the analytical model predicts the general behavior of the clutch; however, the prediction is not accurate due to the above-mentioned unmodeled nonlinear dynamics.

The proposed hybrid LSTM model is effective in modeling the nonlinear dynamics of the clutch and accurately predicts the output torque using fused information from the analytical model and clutch inputs. MSE and mean absolute error for the test data (4 minutes of new data) were determined to be 2.3×10^{-4} N.m and 1.1×10^{-2} N.m, respectively. The proposed hybrid LSTM model also predicts the spikes in the torque due to the instantaneous static friction.

VI. Conclusion

A novel rotary electroadhesive clutch based on segmented electrodes was modeled, designed, and implemented. An analytical model was developed and used in the design optimization. An experimental study was conducted to validate the performance of the proposed segmented design in preventing electroadhesion degradation with time as well as residual adhesion. With the proposed design, a robust torque was achieved for direct current activation signals. A data-driven model augmentation using a hybrid shallow learning approach based on the fusion of the analytical model and an LSTM network was developed. The proposed design for a torque-tunable electroadhesive clutch, along with the data-driven hybrid dynamic model, shows great potential for mobile and wearable HRI systems due to accuracy, high torque density, and low power. Future research will utilize the developed hybrid model in the implementation of an adaptive torque control scheme for application in HRI system.

REFERENCES

[1] N. Feizi, M. Tavakoli, R. V. Patel, and S. F. Atashzar, "Robotics and AI for teleoperation, tele-assessment, and tele-training for surgery in the era of covid-19: Existing challenges, and future vision," *Frontiers in Robotics and AI*, vol. 8, p. 610677, 2021.

[2] I. Díaz, J. J. Gil, and E. Sánchez, "Lower-limb robotic rehabilitation: literature review and challenges," *Journal of Robotics*, vol. 2011, 2011.

[3] P. Maciejasz, J. Eschweiler, K. Gerlach-Hahn, A. Jansen-Troy, and S. Leonhardt, "A survey on robotic devices for upper limb rehabilitation," *Journal of Neuroengineering and Rehabilitation*, vol. 11, no. 1, pp. 1–29, 2014.

[4] A. Mohebbi, "Human-robot interaction in rehabilitation and assistance: a review," *Current Robotics Reports*, vol. 1, no. 3, pp. 131–144, 2020.

[5] T. B. Sheridan, "Human–robot interaction: status and challenges," *Human factors*, vol. 58, no. 4, pp. 525–532, 2016.

[6] S. F. Atashzar, M. Shahbazi, M. Tavakoli, and R. V. Patel, "A grasp-based passivity signature for haptics-enabled human-robot interaction: Application to design of a new safety mechanism for robotic rehabilitation," *International Journal of Robotics Research*, vol. 36, no. 5-7, pp. 778–799, 2017.

[7] A. S. Shafer and M. R. Kermani, "On the feasibility and suitability of mr fluid clutches in human-friendly manipulators," *IEEE/ASME Transactions on Mechatronics*, vol. 16, no. 6, pp. 1073–1082, 2010.

[8] N. Najmaei, A. Asadian, M. R. Kermani, and R. V. Patel, "Design and performance evaluation of a prototype MRF-based haptic interface for medical applications," *IEEE/ASME Transactions on Mechatronics*, vol. 21, no. 1, pp. 110–121, 2015.

[9] J. R. Davidson and H. I. Krebs, "An electrorheological fluid actuator for rehabilitation robotics," *IEEE/ASME Transactions on Mechatronics*, vol. 23, no. 5, pp. 2156–2167, 2018.

[10] S. Pisetskiy and M. Kermani, "High-performance magneto-rheological clutches for direct-drive actuation: Design and development," *Journal of Intelligent Material Systems and Structures*, vol. 32, no. 20, pp. 2582–2600, 2021.

[11] S. Pisetskiy and M. R. Kermani, "A concept of a miniaturized mr clutch utilizing mr fluid in squeeze mode," in *2020 IEEE/RSJ International Conference on Intelligent Robots and Systems (IROS)*, pp. 6347–6352, 2020.

[12] L. Roveda, L. Savani, S. Arlati, T. Dinon, G. Legnani, and L. M. Tosatti, "Design methodology of an active back-support exoskeleton with adaptable backbone-based kinematics," *International Journal of Industrial Ergonomics*, vol. 79, p. 102991, 2020.

[13] J. Guo, J. Leng, and J. Rossiter, "Electroadhesion technologies for robotics: A comprehensive review," *IEEE Transactions on Robotics*, vol. 36, no. 2, pp. 313–327, 2019.

[14] E. W. Schaler, D. Ruffatto, P. Glick, V. White, and A. Parness, "An electrostatic gripper for flexible objects," in *2017 IEEE/RSJ International Conference on Intelligent Robots and Systems (IROS)*, pp. 1172–1179, 2017.

[15] Y. Sun, K. M. Digumarti, H.-V. Phan, O. Aloui, and D. Floreano, "Electro-adhesive tubular clutch for variable-stiffness robots," in *2022 IEEE/RSJ International Conference on Intelligent Robots and Systems (IROS)*, pp. 9628–9634, 2022.

[16] R. Hinchet and H. Shea, "High force density textile electrostatic clutch," *Advanced Materials Technologies*, vol. 5, no. 4, p. 1900895, 2020.

[17] V. Ramachandran, J. Shintake, and D. Floreano, "All-fabric wearable electroadhesive clutch," *Advanced Materials Technologies*, vol. 4, no. 2, p. 1800313, 2019.

[18] S. Diller, C. Majidi, and S. H. Collins, "A lightweight, low-power electroadhesive clutch and spring for exoskeleton actuation," in *2016 IEEE International Conference on Robotics and Automation (ICRA)*, pp. 682–689, 2016.

[19] S. B. Diller, S. H. Collins, and C. Majidi, "The effects of electroadhesive clutch design parameters on performance characteristics," *Journal of Intelligent Material Systems and Structures*, vol. 29, no. 19, pp. 3804–3828, 2018.

[20] D. M. Aukes, B. Heyneman, J. Ulmen, H. Stuart, M. R. Cutkosky, S. Kim, P. Garcia, and A. Edsinger, "Design and testing of a selectively compliant underactuated hand," *International Journal of Robotics Research*, vol. 33, no. 5, pp. 721–735, 2014.

[21] K. Zhang, E. J. Gonzalez, J. Guo, and S. Follmer, "Design and analysis of high-resolution electrostatic adhesive brakes towards static refreshable 2.5 d tactile shape display," *IEEE Transactions on Haptics*, vol. 12, no. 4, pp. 470–482, 2019.

[22] N. Feizi, S. F. Atashzar, M. R. Kermani, and R. V. Patel, "Design and modeling of a smart torque-adjustable rotary electroadhesive clutch for application in human-robot interaction," *IEEE/ASME Transactions on Mechatronics*, (Article in Press), 2023.

[23] N. Feizi, S. F. Atashzar, M. R. Kermani, and R. V. Patel, "Modeling and high-definition control of a smart electroadhesive actuator: Toward application in rehabilitation," *IEEE Transactions on Medical Robotics and Bionics*, vol. 4, no. 4, pp. 1057–1067, 2022.

[24] R. Chen, Z. Zhang, R. Song, C. Fang, D. Sindersberger, G. J. Monkman, and J. Guo, "Time-dependent electroadhesive force degradation," *Smart Materials and Structures*, vol. 29, no. 5, p. 055009, 2020.

[25] T. Nakamura and A. Yamamoto, "Modeling and control of electroadhesion force in dc voltage," *Robomech Journal*, vol. 4, no. 1, pp. 1–10, 2017.

[26] J. Singh, P. A. Bingham, J. Penders, and D. Manby, "Effects of residual charge on the performance of electro-adhesive grippers," in *Annual Conference Towards Autonomous Robotic Systems*, pp. 327–338, 2016.

[27] W. Kalus, Ł. Nagi, and J. Zygarlicki, "Analysis of potential of raising forces acting on electroadhesive pads depending on polarization and supply parameters," *Energies*, vol. 14, no. 9, p. 2517, 2021.

[28] X. Gao, C. Cao, J. Guo, and A. Conn, "Elastic electroadhesion with rapid release by integrated resonant vibration," *Advanced Materials Technologies*, vol. 4, no. 1, p. 1800378, 2019.

[29] H. Xiao, J. Wu, W. Ye, and Y. Wang, "Dynamic modeling for dielectric elastomer actuators based on lstm deep neural network," in *2020 5th International Conference on Advanced Robotics and Mechatronics (ICARM)*, pp. 119–124, 2020.

[30] M. T. Gillespie, C. M. Best, E. C. Townsend, D. Wingate, and M. D. Killpack, "Learning nonlinear dynamic models of soft robots for model predictive control with neural networks," in *2018 IEEE International Conference on Soft Robotics (RoboSoft)*, pp. 39–45, 2018.

[31] T. Luong, K. Kim, S. Seo, J. Jeon, C. Park, M. Doh, J. C. Koo, H. R. Choi, and H. Moon, "Long short term memory model based position-stiffness control of antagonistically driven twisted-coiled polymer actuators using model predictive control," *IEEE Robotics and Automation Letters*, vol. 6, no. 2, pp. 4141–4148, 2021.

[32] S. Hochreiter and J. Schmidhuber, "Long short-term memory," *Neural Computation*, vol. 9, no. 8, pp. 1735–1780, 1997.